International Journal of Ambient Energy

ISSN: (Print) (Online) Journal homepage: https://www.tandfonline.com/loi/taen20

Radiative heat energy exploration on Casson-type nanoliquid induced by a convectively heated porous plate in conjunction with thermophoresis and Brownian movements

MD. Shamshuddin, A. Ghaffari & Usman

To cite this article: MD. Shamshuddin, A. Ghaffari & Usman (2022) Radiative heat energy exploration on Casson-type nanoliquid induced by a convectively heated porous plate in conjunction with thermophoresis and Brownian movements, International Journal of Ambient Energy, 43:1, 6329-6340, DOI: 10.1080/01430750.2021.2014960

To link to this article: https://doi.org/10.1080/01430750.2021.2014960

Published online: 04 Jan 2022.

INTERNATIONAL JOURNAL OF AMBIENT ENERGY
2022, VOL. 43, NO. 1, 6329–6340
https://doi.org/10.1080/01430750.2021.2014960

Taylor & Francis
Taylor & Francis Group

Check for updates

Radiative heat energy exploration on Casson-type nanoliquid induced by a convectively heated porous plate in conjunction with thermophoresis and Brownian movements

MD. Shamshuddin [a], A. Ghaffari[b] and Usman [c]

[a]Department of Mathematics, Vaagdevi College of Engineering (Autonomous), Warangal, India; [b]Department of Mathematics, University of Education, Lahore, Pakistan; [c]Beijing Key Laboratory for Magneto-Photoelectrical Composite and Interface Science, Department of Applied Mathematics, School of Mathematics and Physics, University of Science and Technology Beijing, Beijing 100083, People's Republic of China

ABSTRACT

The interest of this study is to establish a mathematical model and rheological aspects of chemically reacting Casson-type nanofluid flow considering ethylene glycol-based nanoparticles with thermophoretic diffusion and Brownian motion. The basic flow equations are transmuted into non-dimensional form, these dimensionless leading equations are determined to the most excellent potential systematic using some influential similarity transformations with the employment of the Chebyshev Spectral Collocation method. The outcomes for flow rate, temperature, concentration and engineering quantities distribution are shown in terms of graphical presentation. Findings revealed that larger values of Casson fluid parameter lead to suppress velocity as well as fluid temperature. The nanofluid temperature reduces for Brownian motion parameter and enchances for thermophoresis parameter. An increase in Lewis number means a decrease in mass diffusivity resulted in to suppression in fluid concentration. The model results confirmation is tabulated, and the data assessment of the present study with formerly communicated is found excellently accurate.

ARTICLE HISTORY
Received 24 August 2021
Accepted 29 November 2021

KEYWORDS
Thermal radiation; Brownian motion; reactive species; Casson fluid; nanomaterials; thermophoretic diffusion

Nomenclature

Al_2O_3	Alumina nanoparticle
B_0	magnetic field strength
Bi	Biot number
C	species concentration [kg/m^2]
C_f	dimensionless drag force
C_p	specific heat [J/Kg K]
C_w	plate surface concentration
C_∞	ambient nanoparticle concentration
CuO	Copper oxide nanoparticle
D_B	Brownian coefficient [m^2/s]
D_T	Thermophoresis coefficient [m^2/s]
Ec	Eckert number
GO	graphene oxide nanoparticle
Gr	thermal convection number
h_f	thermal transfer coefficient
J_w	concentration gradient rate
k_1	mean absorption coefficient
K_p	porosity term
Kr	chemical reaction parameter
k_{nf}	Maxwell-Garnetts model effective thermal conductivity [Wm^{-1}K^{-1}]
Le	Lewis number
M	magnetic parameter
N	radiation-conduction parameter
Nb	Brownian motion parameter
Nt	Thermophoresis parameter
Nu_x	local Nusselt number
Pr	Prandtl number
q_r	Rosseland approximation of the radiative thermal flux [W/m^2]
q_w	temperature gradient rate
Q	heat generation term
Re_x	local Reynolds number
T	fluid temperature [K]
T_f	convection fluid temperature [K]
T_w	temperature at the wall [K]
T_∞	ambient temperature [K]
u, v	velocity components [m/s]
U_0	plate velocity [m/s]
x	distance along the surface [m]
y	distance normal to surface [m]

Greek symbols

τ	Heat capacity ratio (nanoparticle to base fluid)
τ_w	skin wall drag
β_{nf}	Volumetric thermal expansion of nanofluid
ρ_f	Base fluid density [kg/m^3]
ρ_{nf}	density of nanoparticles [kg/m^3]
$(\rho c_p)_{nf}$	Heat capacity [J/K]
μ_{nf}	Brinkmann effective viscosity [kg m^{-1}s^{-1}]
σ_1	Stefan-Boltzmann constant [Wm^{-2}K^{-4}]
σ_{nf}	electrical conductivity [Ω^{-1}m^{-1}]

CONTACT MD. Shamshuddin shammaths@gmail.com, shamshuddin_md@vaagdevi.edu.in, Usman, usman.malik.ms@gmail.com

ψ	Stream function [m^2/s]
η	similarity variable
θ	dimensionless temperature
φ	dimensionless concentration
ϕ	solid volume fraction

Subscripts

w	quantities at wall
∞	quantities far away from surface
f	base fluid
s	nanoparticle
nf	Nanofluid

1. Introduction

Nanofluids varying in fluctuating streams have plentiful applications in lots of regions such as technological engineering and industrial zones. They establish an exclusive subclass of nanomaterials. The frequently used heat distribution liquids such as engine oil, water and ethylene glycol have little heat conductivity when juxtaposed to metals. Hence, the dispersion of metal solid particles in diffusive heat can significantly raise heat transfer, Nima et al. (2020). Nanoliquids consisting nanosized particles distributed in base liquids, for example, ethylene glycol and water, very imperious characteristics of nanoliquids, are their thermal conductivity power, Ogunseye et al. (2019). The adopted nanoparticles in a synthesis nanofluid are mainly metallic oxides, nitrides, nanotubes carbon, and carbides of diameters ranging from 10 and 100 nm. Pandey and Kumar (2017) considered the nanoliquid Cu-water flow in a slippery and stretchable cylinder with boundary layer heat transfer. Mbambo et al. (2020) experimentally examined nanofluid with ethylene glycol working liquid for the augmentation of heat conductivity of the gold nanosheet graphene. It was sensed that nanoparticle adjusted shape, and the thermal conduction rate is enhanced. Lately, there are emerging first-hand liquids of unique magnetic with super paramagnetic particles (Namanga et al. 2013), which show the property of magnetic and heat augmentation. This case of nanoparticles has extensive usefulness in thin smart films' polymer coating (Kashem et al. 2008), biomedical usages (Issa et al. 2013) and bioconvection swirling nanoliquid (Shamshuddin et al. 2019). Several scholars have presented dynamic mathematical models for the magneto-nanoparticle flow with robust basis experimental data. Rarani, Etesami, and Nasr (2012) applied sonicator-prepared magneto-ethylene glycol iron-oxide nanoliquids to demonstrate that viscous magneto-nanofluid decreased with a higher electric field and that high mass transfer of nanoparticles is observed for high magneto-nanofluid. Kandasamy, Loganathan, and Arasu (2011) obtained nanoliquid closed-form results for wall transpiration influences and stretchable boundary flow. Anwar Bég et al. (2019) carried out a wide study on the different nanoparticles hydromagnetic fluid and base working fluids. They noticed each base fluid combined with silver nanoparticles and achieved the best heat transfer advancement, inductive magnetic and high flow velocity. Furthermore, Raza (2019) considered the Casson fluid stagnation flow in a slippery condition and thermal radiation over a stretching surface. Lund et al. (2019) examined stability analysis for the flow of Casson-type nanofluid over an exponential sheet. Again, Lund et al. (2020) presented dual similarity solutions for Cu–Fe_3O_4/H_2O hybrid nanofluid with the effect of viscous dissipation. Later, Raza et al. (2021) examined the duality and stability of rotating nanofluid on a linear shrinking/stretching sheet employing the Buongiorno model. Humanane, Patil, and Patil (2021) considered the Casson–Williamson nanofluid flow with chemical reaction and thermal radiation over a stretching surface. Rajput et al. (2021) considered Williamson fluid with stagnation point flow with nonlinear thermal radiation over a stretching sheet. Patil, Patil, et al. (2021) examined nano Powell–Eyring fluid near stagnation point with chemical reaction and thermal radiation. Again, Patil, Humane, et al. (2021) examined Prandtl nanofluid flow with chemical reaction and thermal radiation.

The investigation on Brownian motion and thermophoresis with considered stretchable flow medium is of our interest to examine the impacts of the thermofluid terms on the heated vertical plate. The phenomena of thermophoresis are valuable due to non-identical particles rising reaction rate; this occurrence is a result of massive molecules distribution that resulted in complete temperature gradient changes. Brownian moment condition is due to continuous bombardment of atoms in the neighbourhood forum. This form of behaviour is the result of the bombardment of the molecules near the liquid/aeriform as such; the Brownian movement and thermophoresis are significant in engineering sectors. As example, Makinde and Animasaun (2016) considered the thermophoresis and Brownian motion effects on the nonlinear radiative nanofluid and quartic species reaction. Mondal et al. (2019) reported on the numerical solutions of non-Newtonian transient flows through a permeable vertical plate with thermophoresis and Brownian motion impacts. Pakravan and Yaghoubi (2011) carried out a conjectural simulation of the convective nanofluid flow in the presence of thermophoresis and Brownian motion. Kuznetsov and Nield (2014) examined the joint impact of thermophoresis and Brownian movement on the flowing nanofluid in an elongated vertical device. Aminfar and Haghgoo (2012) established a simulation solution for nanoliquid molecules under the influences of thermophoresis and Brownian moment. The observation shows that thermophoresis encouraged molecules carrying in the fluid medium. Such fluids find their applications in chemical mixtures of species transport phenomenon, petrochemical, biotechnology, pharmaceutical and other chemical and technological industries. Numerous scholars anticipated the interesting properties of the nanofluid species mixtures utilising diverse nanoparticles under dissimilar situations, Samrat, Sulochana, and Ashwinkumar (2018) discussed the impacts of chemical mixtures of first-order homogenous magneto-nanomaterial near a stretchable surface for ferrous nanoparticles destructive reactions. Zhang et al. (2015) solved hydromagnetic nanofluid flow utilising the Differential Transform base function method with a chemical reaction with a variable surface heat flux. Qayyum et al. (2017) employed homogenous–heterogeneous reaction effects to Ag-water and Cu-water nanoparticles to forecast the heat propagation potential in a stretching cylinder. The model is implanted with the numerical scheme, and the results are based on the Euler's explicit method, and an agreed quantitative and qualitative computed result is seen. In these reported problems, under convection influence, the reaction is motivated by destructive/generative type of reactive species which has an application in spotting critical parameter value and combustion analysis. Illustrative studies in this area include Salawu et al. (2020), Mishra, Shamshuddin, et al. (2020), Eid et al. (2020), Aleem et al. (2020), and Ullah et al. (2017).

However, to the awareness of the researchers, the thermal transport of nanomaterials over a stretchable plate with different nanoparticles has not been careful and comprehensively examined earlier. There are certain forces in this model that can significantly change the behaviour of the flow, which are carried out by using combined multiphase physical flow characteristics that results in outstanding engineering and industrial outcomes. In light of the aforementioned applications, the novelty of the current study is to investigate Casson-type nanomaterial flow through convectively heated vertical porous plate in the attendance of thermal radiation, thermophoresis and Brownian motion. Thus, the present analysis focusses on extending the studies done in Makinde and Aziz (2011) and Afify and Elgazery (2016). Here, a fixed functional magnetic field is assumed in the extending longitudinally vertical plate direction. By similarity quantities, the nonlinear multi-physical formulation is transformed to ordinary derivatives nonlinear system from partial nonlinear derivatives with appropriate far stream conditions. A numerical alternative with standard technique called the Chebyshev Spectral Collocation scheme is engaged to solve the nonlinear boundary value problem. The method has been reported to have demonstrated a good convergence rate. The used simulation technique is applicable in the nanomagnetic materials technology mechanisms and other fields of science.

2. Physical statement of the problem

Consider the steady 2-dimensional incompressible flow of dissipative and Casson-type nanofluid reaction having different nanoparticles in a heated vertical semi-infinite plate embedded in permeable media examined by imposing novel thermal radiation, thermophoresis and Brownian motion effects. The impact of the magnetic field is examined by taking it normal to the plate. The destructive first-order species mixture properties are homogenous in nature. In the current mathematical modelling design, the physical configuration is shown in Figure 1. The x - coordinate is pulled regarding the moving plate for $a > 0$, the momentum is conjecture to be $u = U_0$. The surface convection and ambient temperature are T_f, T_∞ in particular. C_f and C_∞ denote plate concentration and ambient concentration, and the drift preoccupy in the region $y > 0$ and drift away from the plate in the x - direction by clenching the firm origin and y - axis upended to it. The entire thermo-physical characteristics were presupposed to be invariable of the linearly momentum equations approximated in conformity with the Boussinesq approximations.

It is assumed that the rheological equation of an isotropic and incompressible flow of a Casson fluid can be written as follows:

$$\tau \left. \begin{array}{ll} {}_{ij} = \left\{\mu_b + \dfrac{p_y}{\sqrt{2\pi}}\right\} 2e_{ij} & \text{when } \pi > \pi_c, \\ \tau_{ij} = \left\{\mu_b + \dfrac{p_y}{\sqrt{2\pi_c}}\right\} 2e_{ij} & \text{when } \pi < \pi_c \end{array} \right\} \tag{1}$$

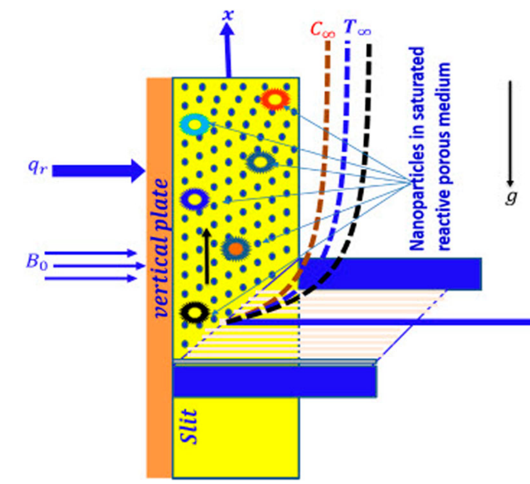

Figure 1. Physical model for continuously moving plate.

Mathematical expression of the yield stress of the fluid is defined as $p_y = \mu_b\sqrt{2\pi}/\gamma$, where μ_b is known as plastic dynamic viscosity of the non-Newtonian fluid, $\pi = e_{ij}e_{ij}$ is the product of the component deformation rate with itself. $\mu = \mu_b + \left\{p_y/\sqrt{2\pi}\right\}$ is assumed as the case of Casson fluid (non-Newtonian) where $\pi > \pi_c$ and π_c are critical values based on the non-Newtonian model. On simplifying p_y and μ, the kinematic viscosity of Casson fluid is defined as follows:

$$\upsilon = \frac{\mu_b}{\rho}\left(1 + \frac{1}{\gamma}\right) \tag{2}$$

The leading equations narrate two-dimensional Casson fluid transportation assuming the above presupposition and extended form the (Makinde and Aziz 2011; Haile and Shankar 2014; Mishra, Pattnaik, et al. 2020).

$$\frac{\partial u}{\partial u} + \frac{\partial v}{\partial y} = 0 \tag{3}$$

$$u\frac{\partial u}{\partial x} + v\frac{\partial u}{\partial y} = \frac{\mu_{nf}}{\rho_{nf}}\left(1 + \frac{1}{\gamma}\right)\frac{\partial^2 u}{\partial y^2} + g\beta_{nf}(T - T_\infty) - \left(\frac{\sigma_{nf}B_0^2}{\rho_{nf}} + \frac{\nu_{nf}}{k_p^*}\right)u \tag{4}$$

$$\left(u\frac{\partial T}{\partial x} + v\frac{\partial T}{\partial y}\right) = \frac{k_{nf}}{(\rho c_p)_{nf}}\left(\frac{\partial^2 T}{\partial y^2}\right) - \frac{1}{(\rho c_p)_{nf}}\left(\frac{\partial q_r}{\partial y}\right) + \frac{\mu_{nf}}{(\rho c_p)_{nf}}\left(1 + \frac{1}{\gamma}\right)\left(\frac{\partial u}{\partial y}\right)^2 + \frac{\sigma_{nf}B_0^2}{(\rho c_p)_{nf}}(u^2) + \tau\left\{D_B\frac{\partial T}{\partial y}\frac{\partial C}{\partial y} + \frac{D_T}{T_\infty}\left(\frac{\partial T}{\partial y}\right)^2\right\} \tag{5}$$

$$\left(u\frac{\partial C}{\partial x} + v\frac{\partial C}{\partial y}\right) = D_B\left(\frac{\partial^2 C}{\partial y^2}\right) + \frac{D_T}{T_\infty}\left(\frac{\partial^2 T}{\partial y^2}\right) - K_r'(C - C_\infty) \tag{6}$$

The applicable initial and frontier constraints are as follows:

$$at\ y = 0:\ u = U_0 = ax, v = 0, -\frac{k_{nf}}{h_f}\frac{\partial T}{\partial y} = (T_f - T), C = C_w$$

$$at\, y \to \infty : u \to 0, T \to T_\infty, C \to C_\infty \tag{7}$$

Here, h_f and T_f are correspondingly connote the thermal transfer coefficient and convection fluid temperature. q_r signifies Rosseland approximation of the radiative thermal flux and is taken from Rosseland (1936) and stand as $\frac{\partial q_r}{\partial y} = -\frac{16\sigma_1 T_\infty^3}{3k_1}\frac{\partial^2 T}{\partial y^2}$ and $\tau = \frac{(\rho c_p)_s}{(\rho c_p)_{nf}}\tau = (\rho c_p)_s/(\rho c_p)_{nf}$ denotes heat capacity ratio of the base fluid nanoparticle, then Equation (3) transforms as follows:

$$u\frac{\partial T}{\partial x} + v\frac{\partial T}{\partial y} = \frac{k_{nf}}{(\rho c_p)_{nf}}\frac{\partial^2 T}{\partial y^2} + \frac{1}{(\rho c_p)_{nf}}\frac{16\sigma_1 T_\infty^3}{3k_1}\frac{\partial^2 T}{\partial y^2} + \frac{\mu_{nf}}{(\rho c_p)_{nf}}\left(1+\frac{1}{\gamma}\right)\left(\frac{\partial u}{\partial y}\right)^2 + \frac{\sigma_{nf} B_0^2}{(\rho c_p)_{nf}}u^2 + \frac{(\rho c_p)_s}{(\rho c_p)_{nf}}\left\{D_B\frac{\partial T}{\partial y}\frac{\partial C}{\partial y} + \frac{D_T}{T_\infty}\left(\frac{\partial T}{\partial y}\right)^2\right\}, \tag{8}$$

Further, ρ_{nf} effective density, $(\rho c_p)_{nf}$ heat capacity, μ_{nf} Brinkmann model effective viscosity and k_{nf} Maxwell-Garnetts model effective thermal conductivity are considered (following Soleimani et al. 2012) and defined as follows:

$$\begin{aligned} \rho_{nf} &= \{(1-\phi)\rho_f + \phi\rho_s\}, \\ \mu_{nf} &= \left\{\frac{\mu_f}{(1-\phi)^{2.5}}\right\}, \\ (\rho c_p)_{nf} &= \{(1-\phi)(\rho c_p)_f + \phi(\rho c_p)_s\}, \\ k_{nf} &= \left\{k_f\left[\frac{k_s + 2k_f - 2\phi(k_f - k_s)}{k_s + 2k_f + 2\phi(k_f - k_s)}\right]\right\} \end{aligned} \tag{9}$$

Following Sheikholeslami and Ganji (2014), σ_{nf} denotes effective electrical conductivity of nanofluid, which is considered as follows:

$$\sigma_{nf} = \sigma_f\left[1 + \frac{3\left(\frac{\sigma_s}{\sigma_f} - 1\right)\phi}{\left\{\left(\frac{\sigma_s}{\sigma_f} + 2\right) - \left(\frac{\sigma_s}{\sigma_f} - 1\right)\phi\right\}}\right] \tag{10}$$

In addition to the above, following Mishra, Pattnaik, et al. (2020), the thermofluid features of various materials are tabulated in Table 1.

Equations (3–7) are streamlined by introducing following (Mishra, Pattnaik, et al. (2020)) transformations

Table 1. Thermofluid features of nanoparticles and working fluid.

	working fluid		Nanoparticles	
Thermofluid features	$C_2H_6O_2$ (Ethylene-glycol)	Al_2O_3 (Alumina)	CuO (Copper Oxide)	GO (Graphene Oxide)
$\rho\,(Kgm^{-3})$	1115	3970	6320	1800
$c_p\,(JKg^{-1}K^{-1})$	2430	765	531.8	717
$k\,(Wm^{-1}K^{-1})$	0.253	40	76.5	5000
$\beta \times 10^{-5}(K^{-1})$	5.7	0.85	1.8	28.4
$\sigma\,(Sm^{-1})$	10.7×10^{-5}	35×10^6	59.5×10^6	1.1×10^{-5}

$$\left.\begin{aligned} &\psi(x,y) = \left(\sqrt{a\nu_f}\right)xf(\eta), \theta(\eta) = \frac{T - T_\infty}{T_f - T_\infty}, \varphi(\eta) = \frac{C - C_\infty}{C_f - C_\infty}, \\ &u = \frac{\partial\psi}{\partial y} = axf'(\eta), v = -\frac{\partial\psi}{\partial x} = -\left(\sqrt{a\nu_f}\right)f(\eta), \eta = y\left(\sqrt{\frac{a}{\nu_f}}\right) \end{aligned}\right\} \tag{11}$$

Using Equations (8–11) on Equations (3)–(7) resulted to below and Equation (3) incidentally confirmed

$$\left(1+\frac{1}{\gamma}\right)f''' + (1-\phi)^{2.5}\left(1-\phi+\phi\frac{\rho_s}{\rho_f}\right)(ff'' - f'^2) + (1-\phi)^{2.5}\left(1-\phi+\phi\frac{\rho_s}{\rho_f}\right)\left(1-\phi+\phi\frac{\beta_s}{\beta_f}\right)Gr\theta - M(1-\phi)^{2.5}\left(1 + \frac{3\left(\frac{\sigma_s}{\sigma_f}-1\right)\phi}{\left\{\left(\frac{\sigma_s}{\sigma_f}+2\right) - \left(\frac{\sigma_s}{\sigma_f}-1\right)\phi\right\}}\right)f' - \frac{1}{K_p}f' = 0 \tag{12}$$

$$\left(\frac{k_{nf}}{k_f} + N\right)\theta'' + \left(1-\phi+\phi\frac{(\rho c_p)_s}{(\rho c_p)_f}\right)\Pr f\theta' + \frac{1}{(1-\phi)^{2.5}}\left(1+\frac{1}{\gamma}\right)\Pr Ecf''^2 + \left(1 + \frac{3\left(\frac{\sigma_s}{\sigma_f}-1\right)\phi}{\left\{\left(\frac{\sigma_s}{\sigma_f}+2\right) - \left(\frac{\sigma_s}{\sigma_f}-1\right)\phi\right\}}\right)\Pr MEcf'^2 + \Pr Nb\theta'\varphi' + \Pr Nt\theta'^2 = 0 \tag{13}$$

$$\varphi'' + \frac{Nt}{Nb}\theta'' + Le\Pr(f\varphi' - Kr\varphi) = 0 \tag{14}$$

The confirming boundary conditions gives

$$\left.\begin{aligned} &f = 0, f' = 1, \theta' = -Bi(1-\theta), \varphi = 1\ at\ \eta = 0 \\ &f' \to 0, h \to 0, \theta \to 0, \varphi \to 0\ when\ \eta \to \infty \end{aligned}\right\} \tag{15}$$

Here, $Gr, M, K_p, \Pr, N, Ec, Q, Nb, Nt, Le, Kr$ and Bi signify thermal convection number, magnetic term, porosity term, Prandtl number, conduction-radiation term, Eckert number, heat generation term, Brownian motion term, thermophoresis term, Lewis number, species mixture term and Biot number, respectively.

The arising dimensionless terms in Equations (12)–(15) are defined as follows:

$$\left.\begin{aligned} &Gr = \frac{g\beta_f(T_f - T_\infty)}{aU_0}, M = \frac{\sigma_f B_0^2}{a\rho_f}, K_p = \frac{k_p^*}{\nu_f}, N = \frac{16\sigma_1}{3k_1 k_f}T_\infty^3, \\ &\Pr = \frac{\nu_f}{\alpha_f}, Ec = \frac{U_0^2}{(c_p)_f(T_f - T_\infty)}, \\ &Nt = \frac{\tau(\rho c_p)_s D_T(T_f - T_\infty)}{(\rho c_p)_f T_\infty \nu_f}, Nb = \frac{\tau(\rho c_p)_s D_B(C_f - C_\infty)}{(\rho c_p)_f \nu_f}, \\ &Le = \frac{\alpha_f}{D_B}, Kr = \frac{K_r^*}{a}, Bi = \frac{h_f}{k_{nf}}\sqrt{\frac{\nu_f}{a}} \end{aligned}\right\} \tag{16}$$

In favour of engineering inquisitiveness, skin wall drag force, temperature gradient rate and concentration gradient rate are

$$\tau_w = -\mu_{nf}\left(\mu_B + \frac{P_y}{\sqrt{2\pi_c}}\right)\left(\frac{\partial u}{\partial y}\right)\bigg|_{y=0},$$

$$\left.\begin{aligned} q_w &= -\left(k_{nf} + \frac{16\sigma_1 T_\infty^3}{3k_1}\right)\left(\frac{\partial T}{\partial y}\right)\bigg|_{y=0}, \\ J_w &= -\ D_B\left(\frac{\partial C}{\partial y}\right)\bigg|_{y=o} \end{aligned}\right\} \tag{17}$$

Therefore, corresponding dimensionless skin wall drag force, Nusselts and mass gradient numbers for flow are as follows:

$$\left.\begin{aligned} C_f &= \frac{2\tau_w}{\rho_f U_0^2}\bigg|_{y=0} \Rightarrow \sqrt{Re_x}(1-\phi)^{2.5}C_f = -2\left(1+\frac{1}{\gamma}\right)f''(0), \\ Nu_x &= \frac{xq_w}{k_f(T_f - T_\infty)} \Rightarrow \frac{Nu_x}{\sqrt{Re_x}} = -\left(\frac{k_{nf}}{k_f} + N\right)\theta'(0), \\ Sh_x &= \frac{xJ_w}{D_B(C_f - C_\infty)} \Rightarrow \frac{Sh_x}{\sqrt{Re_x}} = -\varphi'(0) \end{aligned}\right\} \tag{18}$$

$Re_x = xU_0/\nu_f$ signifies as local Reynolds number.

3. Methodology and results validation

To get the numerical results of Equation (12–14) with boundary conditions (15), the Chebyshev Spectral Collocation method is utilised. To proceed with the numerical procedure, we first introduced some parameters like

$$\begin{aligned} A_1 &= (1-\phi)^{2.5}\left(1-\phi+\phi\frac{\rho_s}{\rho_f}\right), \\ A_2 &= \left(1-\phi+\phi\frac{\beta_s}{\beta_f}\right), \\ A_3 &= \left(1+\frac{3\left(\frac{\sigma_s}{\sigma_f}-1\right)\phi}{\left\{\left(\frac{\sigma_s}{\sigma_f}+2\right)-\left(\frac{\sigma_s}{\sigma_f}-1\right)\phi\right\}}\right), \\ A_4 &= \left(1-\phi+\phi\frac{(\rho c_p)_s}{(\rho c_p)_f}\right) \end{aligned} \tag{19}$$

The equations then take the following form:

$$\left(1+\frac{1}{\gamma}\right)f''' + A_1(ff'' - f'^2) + A_1 A_2 Gr\theta - M(1-\phi)^{2.5}A_3 f' - \frac{1}{K_p}f' = 0 \tag{20}$$

$$\left(\frac{k_{nf}}{k_f}+N\right)\theta'' + A_4 \Pr f\theta' + \frac{1}{(1-\phi)^{2.5}}\left(1+\frac{1}{\gamma}\right)\Pr Ecf''^2 + A_3 \Pr MEcf'^2 + \Pr Q\theta + \Pr Nb\theta'\varphi' + \Pr Nt\theta'^2 = 0 \tag{21}$$

$$\varphi'' + \frac{Nt}{Nb}\theta'' + Le\Pr(f\varphi' - Kr\varphi) = 0 \tag{22}$$

and the associated boundary conditions are

$$\left.\begin{aligned} &f=0, f'=1, \theta' = -Bi(1-\theta), \varphi = 1 \ at\ \eta = 0 \\ &f' \to 0, \theta \to 0, \varphi \to 0 \ when\ \eta \to \infty \end{aligned}\right\} \tag{23}$$

In order to get the differential Equations (20–23) solved, first we converted these equations into linear form with the help of Newton's linearisation approach. For $(i+1)$th iterations, all dependent variables f, θ and φ were replaced by the expressions

$$\begin{aligned} f_{i+1} &= (f_i + \delta f_i), \\ \theta_{i+1} &= (\theta_i + \delta\theta_i), \\ \varphi_{i+1} &= (\varphi_i + \delta\varphi_i), \end{aligned} \tag{24}$$

for all influenced quantities, where δf_i constitutes a very mini swap in f_i. Deploying Equation (24) in (20–22) and relinquishing the quadratic and outrageous-order designations δf_i, $\delta\theta_i$, $\delta\varphi_i$, we derive

$$\begin{aligned} &a_{1,i}\,\delta f''' + a_{2,i}\,\delta f'' + a_{3,i}\,\delta f' + a_{4,i}\,\delta f = R_{1,i} \\ &b_{1,i}\,\delta\theta'' + b_{2,i}\,\delta\theta' + b_{3,i}\,\delta\theta' = R_{2,i} \\ &c_{1,i}\,\delta\varphi'' + c_{2,i}\,\delta\varphi' + c_{3,i}\,\delta\varphi = R_{3,i} \end{aligned} \tag{25}$$

where

$$\begin{aligned} &a_{1,i} = \left(1+\frac{1}{\gamma}\right); \\ &a_{2,i} = A_1 f_i; a_{3,i} = -2A_1 f_i' - M(1-\varphi)^{2.5}A_3 - \frac{1}{k_p}; \\ &a_{4,i} = A_1 f_i'' \end{aligned} \tag{26}$$

$$\begin{aligned} &b_{1,i} = \left(N + \frac{k_{nf}}{k_f}\right); b_{2,i} = A_4 \Pr f_i + \Pr N_b\varphi' + 2\Pr N_t\theta'; \\ &b_{3,i} = \Pr Q \end{aligned} \tag{27}$$

$$c_{1,i} = 1; c_{2,i} = Le\Pr f_i; c_{3,i} = -Kr\,Le\ \Pr \tag{28}$$

and the boundary conditions are

$$\left.\begin{aligned} &\delta f_i = 0 - f_i, \delta f_i' = 1 - f_i', \delta\theta_i' - Bi\,\delta\theta_i = \theta_i' \\ &-Bi(1-\theta_i), \delta\varphi_i = 1 - \varphi_i \ at\ \eta = 0 \\ &\delta f_i' \to 0 - f_i', \delta\theta_i \to 0 - \theta_i, \delta\varphi_i \to 0 - \varphi_i \text{ when } \eta \to \infty \end{aligned}\right\} \tag{29}$$

After the linearisation, we used the Chebyshev Spectral Collocation scheme (Mahmood, Chen, and Ghaffari 2016; Iqbal, Ghaffari, and Mustafa 2019; Mustafa et al. 2019; Ghaffari, Mustafa, and Javed 2018; Majeed et al. 2015) to find the system of equations solution given in (22) with boundary conditions (29). As the spectral method can be used over the finite domain [−1. 1] so that the zone [0, ∞] is first chopped to the discrete zone [0, L] and then by the transformation $\xi_j = 2/L - 1$, the domain [0, L] is converted to [−1, 1]. The grid pints from −1 to 1 are set Gauss-Lobatto collocation points. The derivatives are replaced with the differentiation matrix D with respect to y, which can be determined in various forms, and D is used as assumed by Trefethen (2000). Table 2 symbolises the Nusselt and Sherwood numbers for diverse differences in the main terms. For numerical intentions, it is set up the variables $Le = 1, \Pr = 10, \phi = 0, Q = 0, Ec = 0, Kr = 0, M = 0, K_p \to \infty, Gr = 0, N = 0$. Whereas other parameters are being fixed and speckled over the assortment. We found that our numerical results are best matching with the consequence of Makinde and Aziz (2011), and therefore, we can say confidently that our results are accurate and, hence, Chebyshev Spectral Collocation method code that gives valid results.

Table 2. Comparison of results for $-\theta'(0)$ and $-\varphi'(0)$ when $Le = 1, \Pr = 10, \phi = 0, Q = 0, Ec = 0, Kr = 0, M = 0, K_p \to \infty, Gr = 0, N = 0$ and $Bi \to \infty$.

		$-\theta'(0)$		$-\varphi'(0)$	
Nb	Nt	Results of **Makinde and Aziz (2011)**	Present	Results of **Makinde and Aziz (2011)**	Present
0.1	0.1	0.9524	**0.9524**	2.1294	**2.1294**
0.2	0.1	0.5056	**0.5056**	2.3819	**2.3819**
0.3	0.1	0.2522	**0.2522**	2.4100	**2.4100**
0.4	0.1	0.1194	**0.1194**	2.3997	**2.3996**
0.5	0.1	0.0543	**0.0543**	2.3836	**2.3836**
0.1	0.2	0.6932	**0.6932**	2.2740	**2.2740**
0.1	0.3	0.5201	**0.5201**	2.5286	**2.5286**
0.1	0.4	0.4026	**0.4026**	2.7952	**2.7951**
0.1	0.5	0.3211	**0.3211**	3.0351	**3.0351**

4. Discussion of results

For the discussion tenacity of the impact of different terms on the Casson-type nanofluid flow behaviour under certain assumptions over heated vertical surface, computations have been done for diverse values of $Gr, \gamma, M, K_p, \Pr, N, Kr, Bi, Le$ and for fixed values of other terms on the flow rate f', heat distribution θ and mass distributions φ, which are reported. The engineering quantities such as skin wall friction C_f, temperature gradient Nu and wall mass gradient Sh are also calculated and depicted graphically. A thorough comparison for the nanoparticles (CuO, Al_2O_3, GO) along the non-dimensional similarity variable η is established.

Figures 2 and 3 are schemed to show the impacts of the Casson fluid term γ upon the flow rate and heat transfer fields. Both the profiles and the boundary film viscidness damped along η for growing values of the parameter γ. The rise in the Casson liquid term causes a diminish in the yield stress. In other words, the fluids behave as Newtonian as Casson liquid term rises. As a result, the profiles decreases and this decrease for CuO is slighter larger from Al_2O_3 and GO. The effects of the Grashof number Gr upon flow velocity and heat propagation profiles are depicted in Figures 4 and 5. It is examined that both profiles observe opposite trends, i.e. the velocity field rises but the heat distribution reduces. Because the positivity of the Grashof number behaves as an encouraging pressure gradient that enhances the boundary layer flowing fluid. That is why velocity increases and this increase for GO is on the higher side than from CuO and Al_2O_3. On the other hand, the temperature profile is seen decaying, and this deduction for CuO than from CuO and Al_2O_3. Hence, the upshots of the magnetic parameter M.

The velocity and temperature profiles are shown in Figures 6 and 7. It is noticed from the figures that as the magnetic term is raised, the velocity profiles decline but the temperature field rises. Physically, the higher estimations of the magnetic parameter lead to the Lorentz force's existence, which produces the resistance in the direction of the liquid and, as such, velocity decays. Whereas in the presence of the Lorentz force, more heat energy is generated that causes an increasing temperature profile. Figures 8 and 9 are drawn to predict the influences of the porosity term K_p on the flow rate f' and temperature θ fields. From Figure 8, the velocity profile is witnessed increasing along η for increasing values of the porosity term K_p. The boundary film viscosity rises, and it turns thicker for GO than from Al_2O_3 and

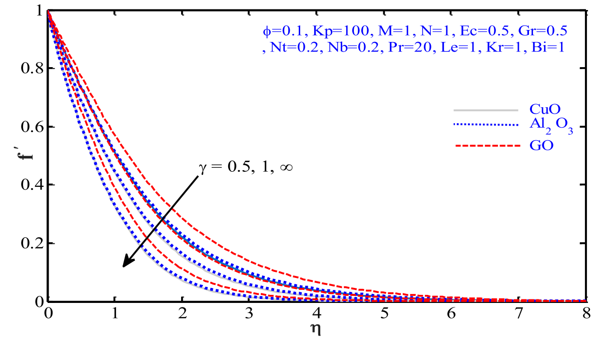

Figure 2. Effects of γ on velocity profile for distinct nanoparticles.

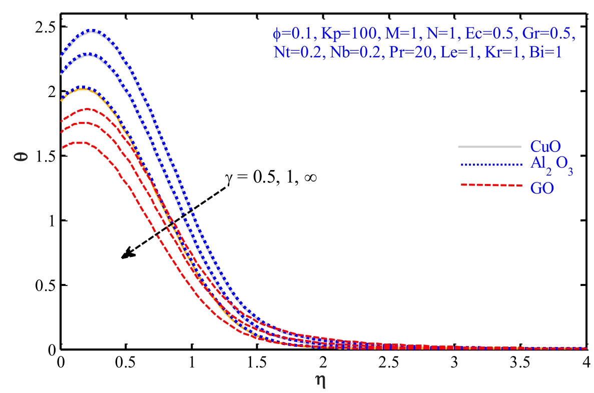

Figure 3. Effects of γ on temperature profile for distinct nanoparticles.

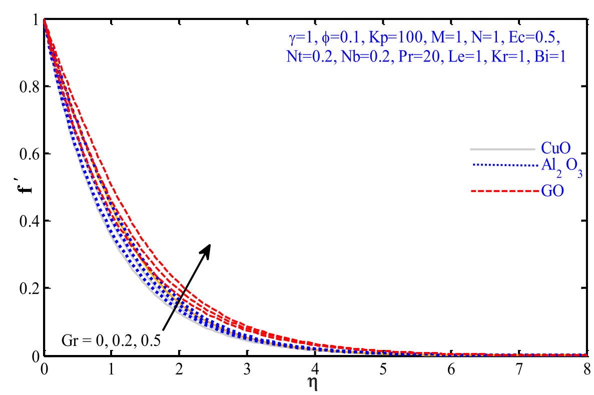

Figure 4. Effects of Gr on velocity profile for distinct nanoparticles.

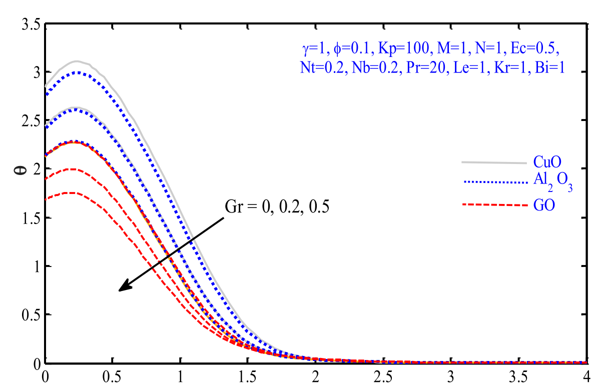

Figure 5. Effects of Gr on temperature profile for distinct nanoparticles.

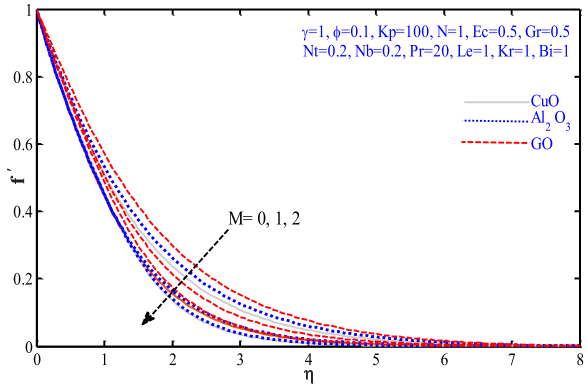

Figure 6. Velocity contours against M for distinct nanoparticles.

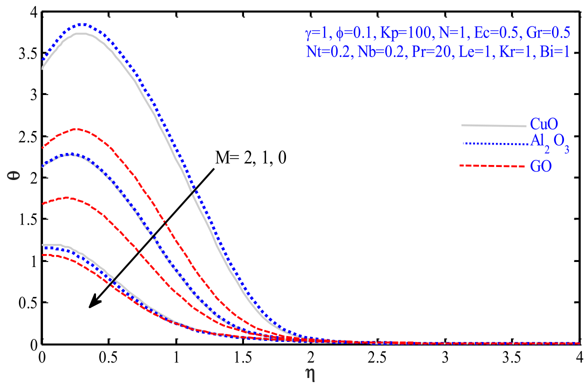

Figure 7. Temperature contours against M for distinct nanoparticles.

CuO The temperature contours in Figure 9 are decreasing along η, and this decrease for *GO* is more considerable. Physically as K_p grows, the resistance reduces, causing the flow to encounter less drag, and as a result, the flow retardation to decrease. Figure 10 elucidates the impacts of the Prandtl number Pr on the heat distribution θ. It is examined that temperature contour is observing cross flow, i.e. increasing near the plate but decreasing abroad from the plate. The parameter Pr is mostly associated with heat and momentum diffusivities. When Pr increases, the thermal diffusivity weakens, allowing momentum diffusivity to dominate thermal diffusivity and, as a result, temperature reduces. Figure 11 deals to estimate the impression of radiation parameter upon temperature profile. Temperature is decaying as the radiation parameter rises, and this deduction for GO is more significant. As due to the dominant effects of the flux at the wall, radiation is found decreasing function of the temperature. The effects of Eckert number *Ec* on the heat field θ are exhibited in Figure 12. Temperature is escalating for high estimations of the Eckert number. The Eckert number demonstrates the effects of heat dissipation impacts. As the Eckert number is raised, the kinetic energy is transformed to heat energy, due to which the thermal conductivity enhances, and as a result, temperature escalates. The increase for Al_2O_3 is more prominent. Figure 13 displays that the concentration field reduces as the Prandtl number Pr enhances. The decrease for CuO,Al_2O_3 and GO is on a similar note. The influences of the Brownian movement term on the heat fields are presented in Figure 14. It can be seen that with the surge in the Brownian movement term, the temperature distribution reduces, and this reduction for GO is larger. Whereas

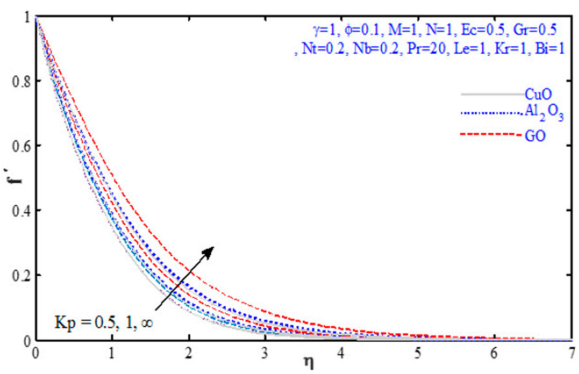

Figure 8. Velocity contours against K_P for distinct nanoparticles.

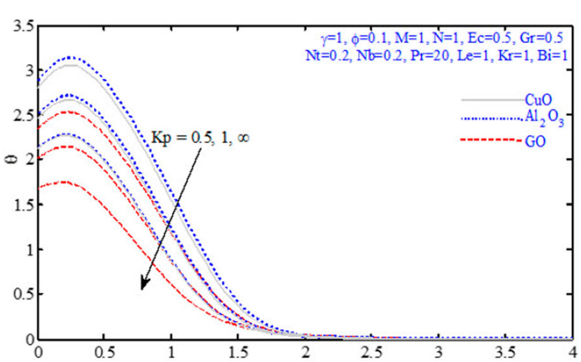

Figure 9. Temperature contours against K_P for distinct nanoparticles.

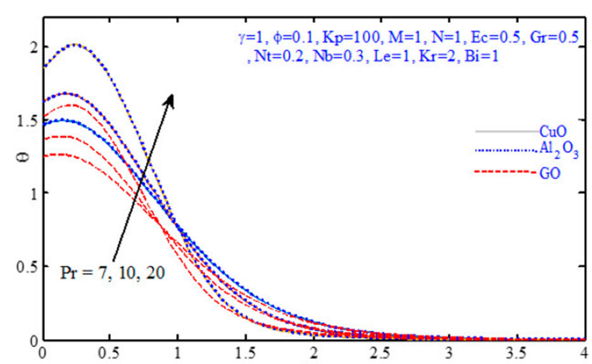

Figure 10. Temperature contours against Pr for distinct nanoparticles.

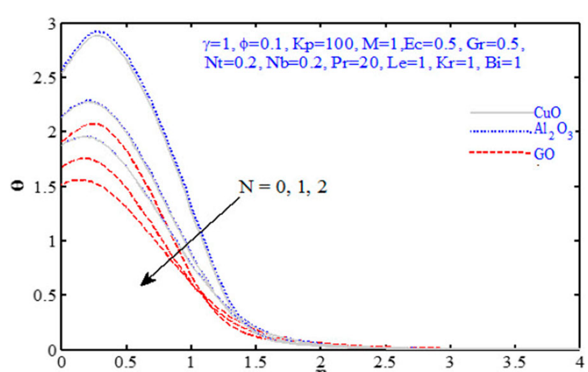

Figure 11. Temperature contours against N for distinct nanoparticles.

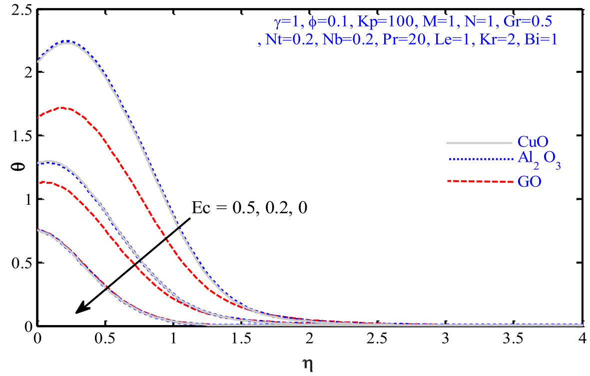

Figure 12. Temperature contours against *Ec* for distinct nanoparticles.

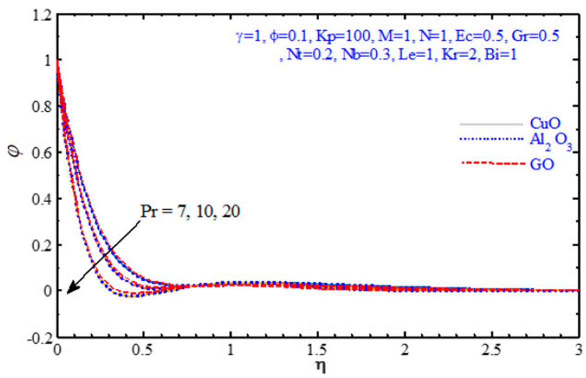

Figure 13. Concentration contours against Pr for distinct nanoparticles.

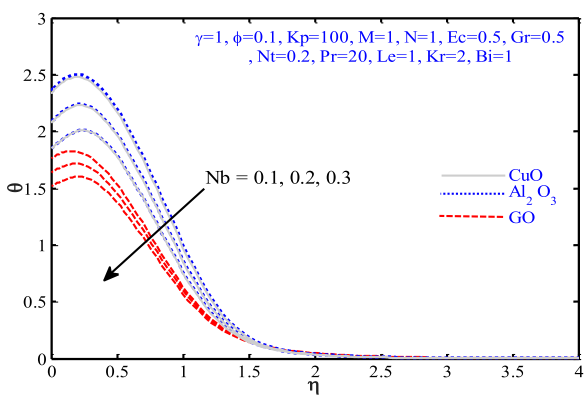

Figure 14. Temperature contours against *Nb* for distinct nanoparticles.

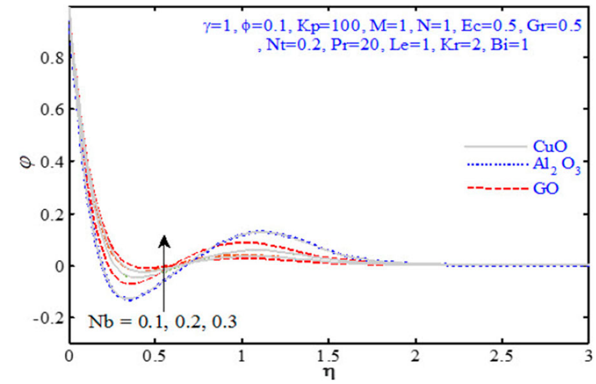

Figure 15. Concentration contours against *Nb* for distinct nanoparticles.

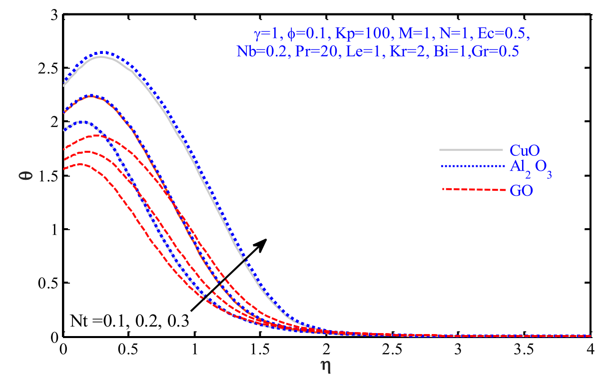

Figure 16. Temperature contours against *Nt* for distinct nanoparticles.

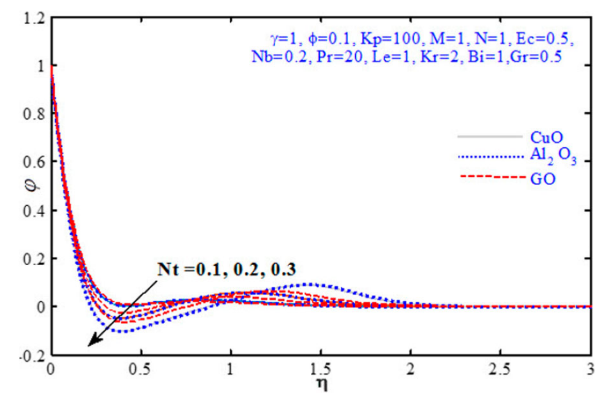

Figure 17. Concentration contours against *Nt* for distinct nanoparticles.

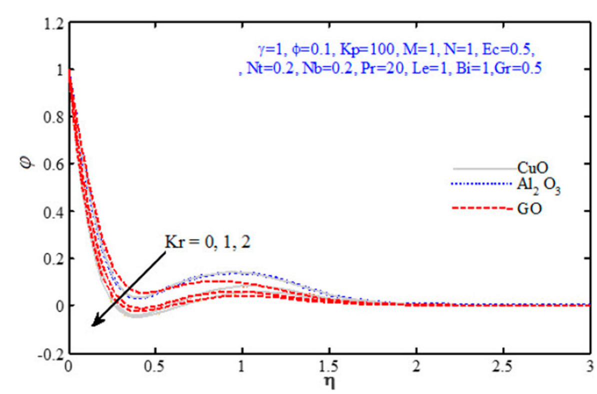

Figure 18. Concentration contours against *Kr* for distinct nanoparticles.

the concentration in Figure 15 is increasing along η. The effects on CuO and Al_2O_3 are more extensive. The temperature profile in Figure 16 is escalating for enlarging values of the thermophoresis parameter. Because during the thermophoresis process, the tiny fluid particles come back from the heated plate to a cool plate, and as a result, a rise in temperature behaviour is noticed. The surge for CuO and Al_2O_3 is more significant than from GO. The impacts of the thermophoresis term on the mass transfer are given in Figure 17. Concentration field is decaying for rising values of the thermophoresis term, and deduction for Al_2O_3 and CuO is more considerable. Figure 18 shows the influences of the chemical reaction term *Kr* on the species mass profile. A noticeable decrement can be predicted from the concentration profile. The larger destructive chemical reaction parameter

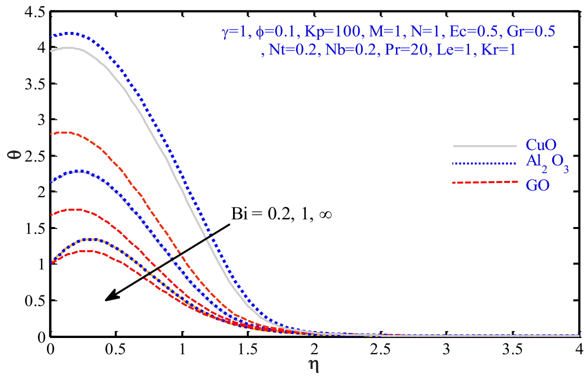

Figure 19. Temperature contours against *Bi* for distinct nanoparticles.

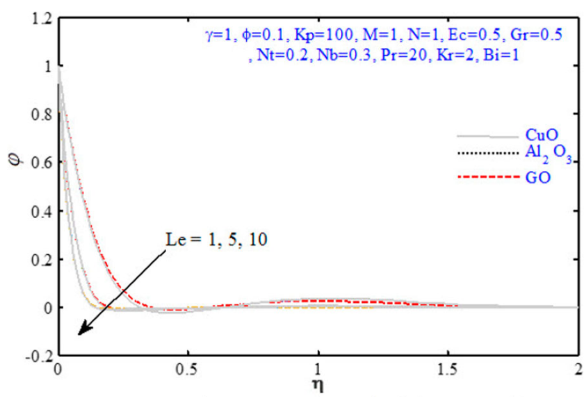

Figure 20. Concentration contours against *Le* for distinct nanoparticles.

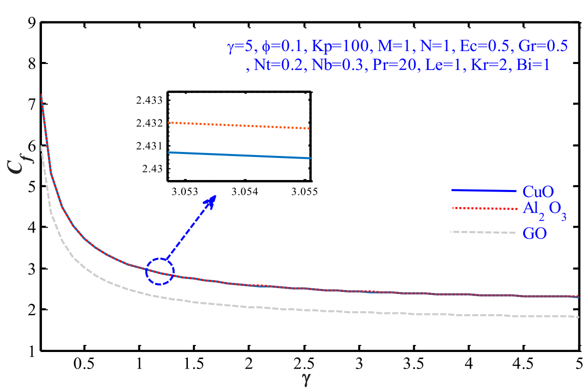

Figure 21. Skin friction variations against γ for distinct nanoparticles.

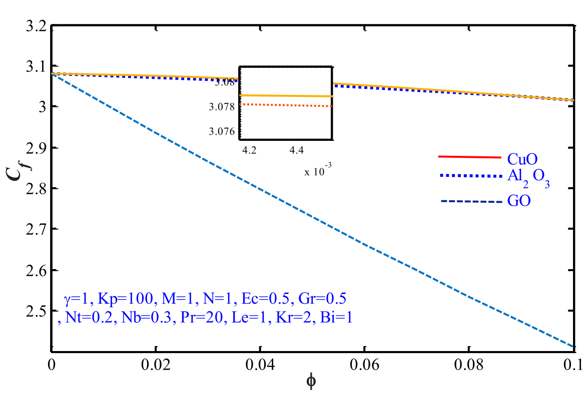

Figure 22. Skin friction variations against ϕ for distinct nanoparticles.

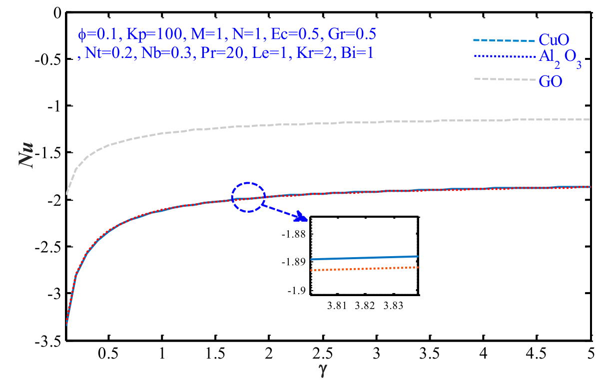

Figure 23. Nusselt number variations against γ for distinct nanoparticles.

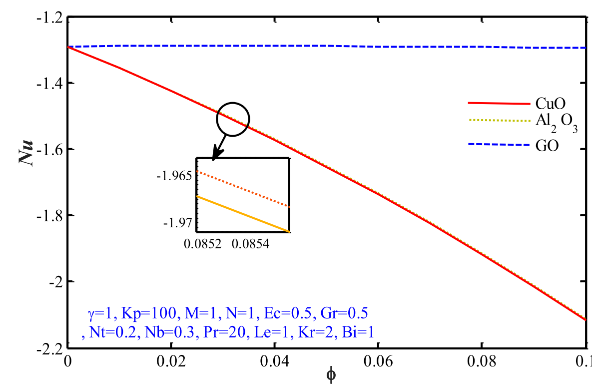

Figure 24. Nusselt number variations against ϕ for distinct nanoparticles.

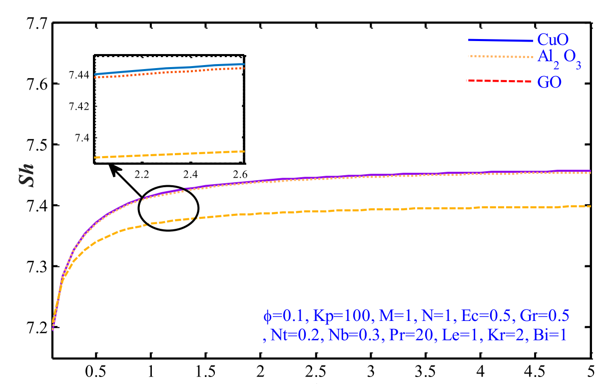

Figure 25. Sherwood number variations against γ for distinct nanoparticles.

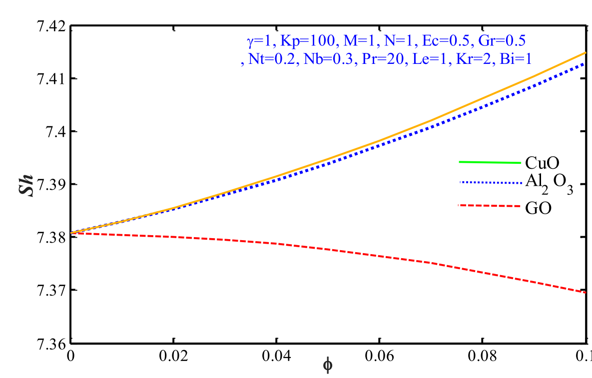

Figure 26. Sherwood number variations against ϕ for distinct nanoparticles.

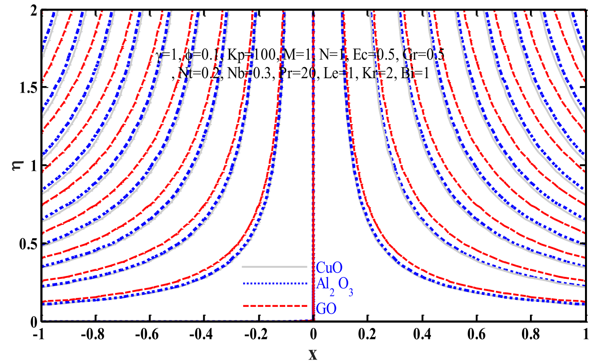

Figure 27. Streamlines for distinct nanoparticles.

leads to a boost in the destructive reaction rate because of which concentration decays. The effects of the Biot number upon concentration profile are shown in Figure 19. It is realised that the profile is plummeting. The reduction for GO is more considerable. Figure 20 demonstrates the impacts of the Lewis number Le on the concentration distribution. The mass profile is decreasing along with η for expanding values of the Lewis number Le. The increase in the Lewis number owns a weaker Brownian motion coefficient, and as a result, concentration decays. The coefficient wall dragging C_f against the Casson fluid parameter γ for distinct nanoparticles is plotted in Figure 21. Similarly, the coefficient skin resistance C_f along with volume fraction parameter ϕ for distinct nanoparticles is presented in Figure 22. The Nusselt local number is schemed along with the Casson fluid parameter γ and volume fraction parameter ϕ in Figures 23 and 24 for distinct nanoparticles. Also, the local Sherwood number alongside the Casson liquid term γ and the fractional volume parameter ϕ for distinct nanoparticles is shown in Figures 25 and 26. The stream lines are drawn in Figures 27 and 28 to predict the flow behaviour.

5. Conclusion

A mathematical model has been developed for chemical reacting Casson-type nanofluid flow by considering ethylene glycol-based nanoparticles. The rheological aspects are studied in occupancy of novel thermophoretic diffusion, Brownian movement, radiative terms and reactive species. CSCM (Chebyshev Spectral Collocation Method) is employed to examine the effects of the physical parameters upon boundary layer profiles. Thus, following conclusion can be drawn:

- The velocity of the fluid decreases for the Casson fluid parameter, magnetic parameter but increases for the Grashof number and porosity parameter.
- The fluid temperature decays for Casson fluid parameter, Grash of number, porosity parameter, radiation parameter, Eckert number and Biot number.
- For magnetic parameter and Prandtl number the fluid temperature enhances.

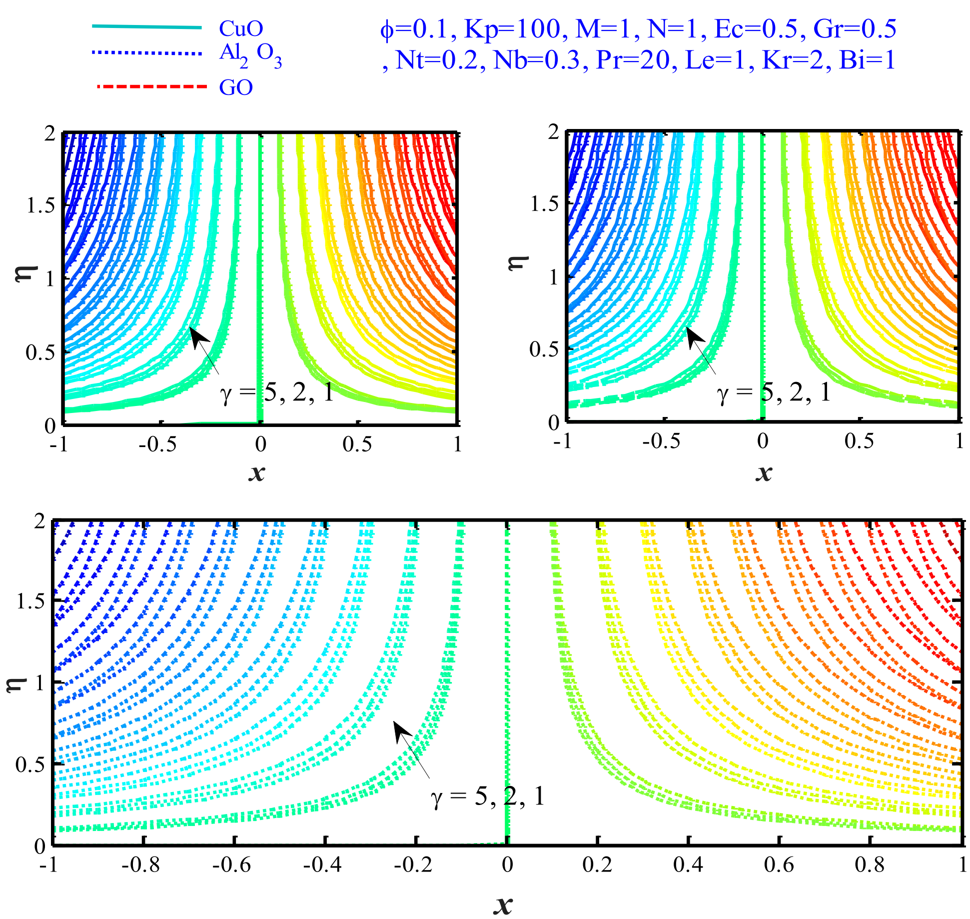

Figure 28. Casson fluid Streamlines for distinct nanoparticles.

- The nanofluid temperature is reducing for *Nb* whereas it escalates for *Nt*.
- The nanoparticles concentration reduces for Pr, *Nt*, *Kr* and *Le* whereas enhances for *Nb*.

The study finds its usefulness in medical sciences, material sciences, biotechnology, and so on. As such, further extension of the study is encouraged by incorporating different metal nanoparticles in an annular cylinder.

Disclosure statement

No potential conflict of interest was reported by the author(s).

Funding

This work is partially supported by the National Natural Science Foundation of China [Nos. 11771040 and 11861131004] and the Fundamental Research Funds for the central universities [No. 06500073].

ORCID

MD. Shamshuddin http://orcid.org/0000-0002-2453-8492
Usman Malik http://orcid.org/0000-0002-5989-3670

References

Afify, A. A., and N. S. Elgazery. 2016. "Effect of a Chemical Reaction on Magnetohydrodynamic Boundary Layer Flow of a Maxwell Fluid Over a Stretching Sheet with Nanoparticles." *Particuology* 29: 154–161.

Aleem, M., M. I. Asjad, A. Shaheen, and I. Khan. 2020. "MHD Influence on Different Water Based Nanofluids (TiO_2, Al_2O_3, CuO) in Porous Medium with Chemical Reaction and Newtonian Heating." *Choas, Solitons & Fractals* 130: 109437. doi:10.1016/j.choas.2019.109437.

Aminfar, H., and M. R. Haghgoo. 2012. "Brownian Motion and Thermophoresis Effects on Natural Convection of Alumina-Water Nanofluid." *Proceedings of the IMchE-Part C: Journal of Mechanical Engineering and Science* 227 (1): 100–110.

Anwar Bég, O., S. Kuharat, M. Ferdows, M. Das, A. Kadir, and MD. Shamshuddin. 2019. "Modelling Magnetic Nanopolymer Flow with Magnetic Induction and Nanoparticle Solid Volume Fraction Effects: Solar Magnetic Nanopolymer Fabrication Simulation." *Proceedings of the IMechE-Part N: Journal of Nanomaterial, Nanoengineering and Nanosystems* 233 (1): 27–45.

Eid, M. R., K. L. Mahny, A. Dar, and T. Muhammad. 2020. "Numerical Study for Carreau Nanofluid Flow Over a Convectively Heated Nonlinear Stretching Surface with Chemically Reactive Species." *Physica A: Statistical Mechanics and its Applications* 540: 123063. doi:10.1016/j.physa.2019.123063.

Ghaffari, A., I. Mustafa, and T. Javed. 2018. "Time Dependent Convective Non-Orthogonal Hiemenz Flow of Viscoelastic Walter's B Fluid Towards a Non-Uniformly Heated Vertical Surface: Using Spectral Method." *Nihon Reoroji Gakkaishi* 46 (4): 155–164.

Haile, E., and B. Shankar. 2014. "Heat and Mass Transfer Through a Porous Media of MHD Flow of Nanofluids with Thermal Radiation, Viscous Dissipation and Chemical Reaction Effects." *American Chemical Science Journal* 4 (6): 828–846. doi:10.1016/j.cplett.2020.13801.

Humane, P. P., V. S. Patil, and A. B. Patil. 2021. "Chemical Reaction and Thermal Radiation Effects on Magnetohydrodynamics Flow of Casson-Williamson Nanofluid Over a Porous Stretching Surface." *Proceedings of the Institution of Mechanical Engineers, Part E: Journal of Process Mechanical Engineering* 235 (6): 2008–2018.

Iqbal, M., A. Ghaffari, and I. Mustafa. 2019. "Investigation into Thermophoresis and Brownian Motion Effects of Nanoparticles on Radiative Heat Transfer in Hiemenz Flow Using Spectral Method." *Scientia Iranica* 26 (6): 3905–3916.

Issa, B., I. M. Obaidat, B. A. Albiss, and Y. Haik. 2013. "Magnetic Nanoparticles: Surface Effects and Properties Related to Biomedicine Applications." *International Journal of Molecular Science* 14 (11): 21266–21305.

Kandasamy, R., P. Loganathan, and P. P. Arasu. 2011. "Scaling Group Transformation for MHD Boundary-Layer Flow of a Nanofluid Past a Vertical Stretching Surface in the Presence of Suction/Injection." *Nuclear Engineering Design* 241 (6): 2053–2059.

Kashem, M. M. A., J. Perlich, L. Schulz, S. V. Roth, and P. Muiller-Buschbaum. 2008. "Correlated Roughness in Polymer Films Containing Maghemite Nanoparticles." *Macromolecules* 41: 2186–2194.

Kuznetsov, A. V., and D. A. Nield. 2014. "Natural Convective Boundary Layer Flow of a Nanofluid Past a Vertical Plate: A Revised Model." *International Journal of Thermal Science* 77: 126–129.

Lund, L. A., Z. Omar, I. Khan, J. Raza, M. Bakouri, and I. Tlili. 2019. "Stability Analysis of Darcy-Forchheimer Flow of Casson Type Nanofluid Over an Exponential Sheet: Investigation of Critical Points." *Symmetry* 11 (3): 412. doi:10.3390/sym11030412.

Lund, L. A., Z. Omar, J. Raza, and I. Khan. 2020. "Magnetohydrodynamic Flow of Cu–Fe_3O_4/H_2O Hybrid Nanofluid with Effect of Viscous Dissipation: Dual Similarity Solutions." *Journal of Thermal Analysis and Calorimetry* 2: 915–927.

Mahmood, A., B. Chen, and A. Ghaffari. 2016. "Hydromagnetic Hiemenz Flow of Micropolar Fluid Over a Nonlinearly Stretching/Shrinking Sheet: Dual Solutions by Using Chebyshev Spectral Newton Iterative Scheme." *Journal of Magnetism and Magnetic Materials* 416: 329–334.

Majeed, A., T. Javed, A. Ghaffari, and M. M. Rashidi. 2015. "Analysis of Heat Transfer due to Stretching Cylinder with Partial Slip and Prescribed Heat Flux: A Chebyshev Spectral Newton Iterative Scheme." *Alexandria Engineering Journal* 54 (4): 1029–1036.

Makinde, O. D., and I. L. Animasaun. 2016. "Thermophoresis and Brownian Motion Effects on MHD Bioconvection of Nanofluid with Nonlinear Thermal Radiation and Quartic Chemical Reaction Past an Upper Horizontal Surface of a Paraboloid of Revolution." *Journal of Molecular Liquids* 221: 733–743.

Makinde, O. D., and A. Aziz. 2011. "Boundary Layer Flow of a Nanofluid Past a Stretching Sheet with a Convective Boundary Condition." *International Journal of Thermal Science* 50: 1326–1332.

Mbambo, M. C., M. J. Madito, T. Khamliche, C. B. Mtshali, Z. M. Khumalo, I. G. Madiba, B. M. Mothudi, and M. Maaza. 2020. "Thermal Conductivity Enhancement in Gold Decorated Graphene Nanosheets in Ethylene Glycol Based Nanofluid." *Scientific Reports* 10: 14730. doi:10.1038/s41598-020-71740-1.

Mishra, A. K., P. K. Pattnaik, S. R. Mishra, and N. Senapati. 2020. "Dissipative Heat Energy on Cu and $A_{l2}O_3$ Ethylene-Glycol-Based Nanofluid Flow Over a Heated Semi-Infinite Vertical Plate." *Journal of Thermal Analysis and Calorimetry* 145: 129–137.

Mishra, S. R., MD. Shamshuddin, O. Anwar Beg, and A. Kadir. 2020. "Adomain Computation of Radiative-Convective bi-Directional Stretching Flow of a Magnetic non-Newtonian Fluid in Porous Media with Homogenous-Heterogeneous Reactions." *International Journal of Modern Physics B* 34 (18): 2050165. doi:10.1142/S021797922001659..

Mondal, M., R. Biswas, K. Shanchia, M. Hasan, and S. F. Ahmmed. 2019. "Numerical Investigation with Stability Convergence Analysis of Chemically Hydromagnetic Casson Nanofluid Flow in the Effects of Thermophoresis and Brownian Motion." *International Journal of Heat and Technology* 37 (1): 59–70.

Mustafa, I., T. Javed, A. Ghaffari, and H. Khalil. 2019. "Enhancement in Heat and Mass Transfer Over a Permeable Sheet with Newtonian Heating Effects on Nanofluid: Multiple Solutions Using Spectral Method and Stability Analysis." *Pramana* 93 (4): 53. doi:10.1007/s12043-019-1814-3.

Namanga, J., J. Foba, D. T. Ndinteh, D. M. Yufanyi, and R. W. M. Krause. 2013. "Synthesis and Magnetic Properties of Superparamagnetic Nanocomposite Pectin-Magnetite Nanocomposite." *Journal of Nanomaterials* 2013: 137275. doi:10.1155/2013/137275.

Nima, N. I., S. O. Salawu, M. Ferdows, M. D. Shamshuddin, A. Alsenafi, and A. Nakayama. 2020. "Melting Effect on Non-Newtonian Fluid Flow in Gyrotactic Microorganism Saturated Non-Darcy Porous Media with Variable Fluid Properties." *Applied Nanoscience* 10: 3911–3924.

Ogunseye, H. A., S. O. Salawu, Y. O. Tijani, M. Riliwan, and P. Sibanda. 2019. "Dynamical Analysis of Hydromagnetic Brownian and Thermophoresis Effects of Squeezing Eyring-Powell Nanofluid Flow with Variable Thermal Conductivity and Chemical Reaction." *Multidiscipline Modeling and Material Structures* 15 (6): 1100–1120.

Pakravan, H. A., and M. Yaghoubi. 2011. "Combined Thermophoresis, Brownian Motion and Dufour Effects on Natural Convection of Nanofluids." *International Journal of Thermal Science* 50 (3): 394–402.

Pandey, A. K., and M. Kumar. 2017. "Boundary Layer Flow and Heat Transfer Analysis on Cu-Water Nanofluid Flow Over a Stretching Cylinder with Slip." *Alexandria Engineering Journal* 56 (4): 671–677.

Patil, A. B., P. P. Humane, V. S. Patil, and G. R. Rajput. 2021. "MHD Prandtl Nanofluid Flow due to Convectively Heated Stretching Sheet Below the Control of Chemical Reaction with Thermal Radiation." *International Journal of Ambient Energy*. doi:10.1080/01430750.2021.1888803.

Patil, V. S., A. B. Patil, S. Ganesh, P. P. Humane, and N. S. Patil. 2021. "Unsteady MHD Flow of a Nano Powell-Eyring Fluid Near Stagnation Point Past a Convectively Heated Stretching Sheet in the Existence of Chemical Reaction with Thermal Radiation." *Materials Today: Proceedings* 44: 3767–3776.

Qayyum, S., M. I. Khan, T. Hayat, and A. Alsaedi. 2017. "A Frame Work for Nonlinear Thermal Radiation and Homogenous-Heterogeneous Reactions Flow Based on Silver-Water and Copper-Water Nanoparticles: A Numerical Model for Probable Error." *Results in Physics* 7: 1907–1914.

Rajput, G. R., B. P. Jadhav, V. S. Patil, and S. N. Salunkhe. 2021. "Effects of Nonlinear Thermal Radiation Over Magnetized Stagnation Point Flow of Williamson Fluid in Porous Media Driven by the Stretching Sheet." *Heat Transfer* 50 (3): 2543–2557.

Rarani, E. M., N. Etesami, and E. M. Nasr. 2012. "Influence of the Uniform Electric Field on Viscosity of Magnetic Nanofluid (Fe_3O_4-EG)." *Journal of Applied Physics* 112 (9): 094903. doi:10.1063/1.4763469.

Raza, J. 2019. "Thermal Radiation and Slip Effects on Magnetohydrodynamic (MHD) Stagnation Point Flow of Casson Fluid Over a Convective Stretching Sheet." *Propulsion and Power Research* 8 (2): 138–146.

Raza, J., S. Dero, L. A. Lund, and Z. Omar. 2021. "Duality and Stability of MHD Darcy–Forchheimer Porous Medium Flow of Rotating Nanofluid on a Linear Shrinking/Stretching Sheet: Buongiorno Model." *International Journal of Numerical Methods for Heat & Fluid Flow*. doi:10.1108/HFF-01-2021-0054.

Rosseland, S. 1936. *Theoretical Astrophysics*. New York: Oxford University.

Salawu, S. O., R. A. Kareem, MD. Shamshuddin, and S. U. Khan. 2020. "Double Exothermic Reaction of Viscous Dissipative Oldroyd-8 Constant Fluid and Thermal Ignition in a Channel." *Chemical Physics Letters* 760: 100732.

Samrat, S. P., C. Sulochana, and G. P. Ashwinkumar. 2018. "Impact of Thermal Radiation and Chemical Reaction on Unsteady 2D Flow of Magnetic-Nanofluids Over an Elongated Plate Embedded with Ferrous Nanoparticles." *Frontiers in Heat and Mass Transfer* 10: 31. doi:10.5098/hmt.10.31.

Shamshuddin, MD., S. R. Mishra, O. Anwar Bég, and A. Kadir. 2019. "Adomain Decomposition Method Simulation of Von Karman Swirling Bioconvection Nanofluid Flow." *Journal of Central South University* 26 (10): 2797–2813.

Sheikholeslami, M., and D. D. Ganji. 2014. "Ferrohydrodynamic and Magnetohydrodynamic Effects on Ferrofluid Flow and Convective Heat Transfer." *Energy* 75: 400–410.

Soleimani, S., M. Sheikholeslami, D. D. Ganji, and M. Gorji-Bandpay. 2012. "Natural Convection Heat Transfer in a Nanofluid Filled Semi-Annulus Enclosure." *International Journal of Heat and Mass Transfer* 39: 565–574.

Trefethen, L. N. 2000. *Spectral Methods in MATLAB*. Philadelphia: Society for Industrial and Applied Mathematics.

Ullah, I., S. Shafie, O. D. Makinde, and I. Khan. 2017. "Unsteady MHD Falkner-Skan Flow of Casson Nanofluid with Generative/Destructive Chemical Reaction." *Chemical Engineering Science* 173: 694–706.

Zhang, C., L. Zheng, X. Zhang, and G. Chen. 2015. "MHD Flow and Radiation Heat Transfer of Nanofluids in Porous Media with Variable Heat Flux and Chemical Reactions." *Applied Mathematics and Modelling* 39 (1): 165–181.